What is the cause(s) of positive ozone trends in three megacity clusters in eastern China during 2015–2020?

Tingting Hu[1], Yu Lin[1], Run Liu[1,2], Yuepeng Xu[1], Boguang Wang[1,2], Yuanhang Zhang[3], Shaw Chen Liu[1,2]

[1]Institute for Environmental and Climate Research, Jinan University, Guangzhou, 511443, China
[2]Guangdong-Hongkong-Macau Joint Laboratory of Collaborative Innovation for Environmental Quality, Guangzhou, 511443, China
[3]State Key Joint Laboratory of Environmental Simulation and Pollution Control, College of Environmental Sciences and Engineering, Peking University, Beijing, 100871, China

Correspondence to: Run Liu (liurun@jnu.edu.cn), Shaw Chen Liu (shawliu@jnu.edu.cn)

Abstract. Due to a robust emission control policy, significant reductions in major air pollutants, such as $PM_{2.5}$, SO_2, NO_2, and CO, were observed in China between 2015 to 2020. On the other hand, during the same period, there was a notable increase in ozone (O_3) concentrations, making it a prominent air pollutant in eastern China. The annual mean concentration of maximum daily 8-hour average (MDA8) O_3 exhibited alarming linear trends of 2.4, 1.1, and 2.0 ppb yr^{-1} in three megacity clusters: Beijing-Tianjin-Hebei (BTH), Yangtze River Delta (YRD) and Pearl River Delta (PRD~~).~~), respectively. Additionally, there was a significant three-fold increase in the number of O_3-exceeding days, defined as MDA8 O_3>75 ppb during the same period. Our analysis indicated that the upward trends in the annual mean concentration of MDA8 were primarily driven by the rise in consecutive O_3-exceeding days. Furthermore, from 2015 to 2017, there was a widespread expansion of high O_3 concentrations from urban centers to surrounding rural regions, resulting in a more uniform spatial distribution of O_3 after 2017. Lastly, we ~~discovered~~found a close association between O_3 episodes ~~featuring~~with four or more consecutive O_3-exceeding days and the position and strength of tropical cyclones (TCs) in the northwest Pacific and the West Pacific subtropical high (WPSH). The TC and WPSH contributed to meteorological conditions characterized by clear skies, subsiding air motion, high vertical stability in the lower troposphere, increased solar radiation, and positive temperature anomaly at the surface. These favorable meteorological conditions greatly facilitated the formation of O_3. Thus, we propose that the worsening O_3 trends observed in BTH, YRD and PRD from 2015 to 2020 can be mostly attributed to enhanced photochemical O_3 production resulting from an increased occurrence of meteorological conditions with high solar radiation and positive temperature anomalies under the influence of WPSH and ~~tropical cyclones~~TCs.

1 Introduction

Ozone (O_3) is an important greenhouse gas, which can also have adverse effects on human health, vegetation, and materials (Bell et al., 2006; Cohen et al., 2017; Kalabokas et al., 2020; Nuvolone et al., 2018). Surface O_3 is a secondary pollutant produced by photochemical reactions involving O_3 precursors such as volatile organic compounds (VOCs), carbon monoxide

(CO) and nitrogen oxides (NOx) (Ma et al., 2012; Monks et al., 2015; Wang et al., 2017). ~~Compared~~In addition to O_3 precursors, meteorological conditions are also crucial factors driving the O_3 formation. Solar radiation, temperature, relative humidity, wind speed, and cloud cover have been found to be closely related to O_3 formation (Dong et al., 2020; Han et al., 2020; Yin et al., 2019). ~~In addition~~Furthermore, large-scale circulations, such as the East Asian monsoon, West Pacific subtropical high (WPSH) and tropical cyclones (TCs) can influence O_3 concentration as well (Lu et al., 2019; Rowlinso et al., 2019; Yang et al., 2014; Zhao and Wang, 2017).

The concentrations of air pollutants SO_2, NOx, CO, PM_{10} and $PM_{2.5}$ in China have been significantly reduced since 2013 (Li M. et al., 2021; Li et al., 2022; Zhai et al., 2019), thanks to the implementation of "Air Pollution Prevention and Control Action Plan". However, the O_3 concentration has dramatically increased and emerged as a major air pollutant in eastern China (Bian et al., 2019; Fu et al., 2019; Wang et al., 2020; Zheng et al., 2018). O_3 concentrations are particularly high in the three megacity clusters in eastern China, namely Beijing-Tianjin-Hebei (BTH), Yangtze River Delta (YRD) and Pearl River Delta (PRD) (Gao et al., 2020; Guo et al., 2019; Li K. et al., 2021; Liu et al., 2018; Yang et al., 2019).

Annual mean concentrations of maximum daily 8-hour average (MDA8) O_3 in the three megacity clusters are shown in Fig. 1. The linear increasing trends of MDA8 O_3 for BTH, YRD and PRD are 2.4, 1.1 and 2.0 ppb yr^{-1}, respectively during the period 2015–2020. These trends are unusually large compared to the trends in other parts of China as well as the trends worldwide (Chen et al., 2020; Lu et al., 2018; Professional Committee of Ozone Pollution Control of Chinese Society for Environmental Sciences, 2022; Zhang et al., 2020). Thus, a crucial scientific question is: What is the cause(s) of these large positive trends in O_3 concentration? Some recent studies suggested that changing photochemical processes induced by anthropogenic emissions are responsible for these trends (Li et al., 2019; Li et al., 2022; Shao et al., 2021; Wang et al., 2020). However, in our analysis of the O_3 trends at individual stations in eastern China during the period 2015–2020, we noticed that the interannual variations of O_3 concentration were strongly affected by the position and intensity of WPSH and the presence of TCs in the western Pacific and South China Sea, consistent with the results of a number of recent studies (Chang et al., 2019; Mao et al., 2020; Ouyang et al., 2022; Zhao and Wang, 2017).These results suggest that transport/meteorological parameters associated with WPSH and TCs may also play an important role in the large trends of MDA8 O_3.

The significant impact of WPSH on weather patterns and O_3 concentrations over East China is widely recognized (Bachmann, 2015; Chang et al., 2019; Yin et al., 2019; Zhao and Wang, 2017). It is well established that the WPSH plays a critical role in controlling weather conditions, which in turn affects O_3 concentrations. For example, the WPSH is known to contribute to the formation of the East Asian monsoon and influence precipitation patterns in the YRD. ~~Furthermore, it~~It also influences air temperature and precipitation across North and South China (Zhang, 2001; Zhao and Wang, 2017). These changes in meteorological conditions have a profound impact on the photochemical ~~formation~~production, dispersion, and accumulation of O_3.

Previous studies have indicated that in the ~~outer regions~~peripheries of TCs, PRD experiences specific atmospheric conditions, e.g., high pressure, low humidity, and intense solar radiation~~.~~, which are highly conducive to O_3 formation. These conditions often result in consecutive days with elevated levels of O_3, as observed in various case studies (Ouyang et al., 2022; Wei et al., 2016). Furthermore, statistical investigations have established several noteworthy connections between TCs and O_3 concentrations in the PRD area. For example, the meteorological conditions associated with the TC periphery frequently contributed to the formation of elevated surface O_3 levels and aerosols (Deng et al., 2019). In addition, TCs in the East China Sea had a higher likelihood of causing increased O_3 concentrations in the PRD region (Zhao et al., 2022). Lastly, TCs in the vicinity of Taiwan, China have the greatest influence on air quality in Hong Kong when compared to TCs in other areas, which is primarily because these TCs facilitate the transportation of air pollutants from the PRD region (Lam et al., 2018).

In this study, we focus on exploring possible contributions to the large positive O_3 trends in the three megacity clusters in eastern China by changes in meteorological parameters associated with WPSH and TCs during the period 2015–2020. ~~This~~The rest of this paper is organized as follows. In Section 2, the data and methodology used in this study are described. Major characteristics of the O_3 interannual variability and trends in the three megacity clusters are discussed in Section 3.1. In Section 3.2, we examine the spatial expansion and ~~quasi-~~saturation of high O_3. The annual change of O_3-exceeding days with different durations are also examined. A hypothesis of the cause of O_3 trends in three megacity clusters in eastern China during 2015–2020 is presented in Section 3.3. Section 4 presents a summary and conclusions.

2 Data and methodology

2.1 Pollutant Data

~~In this study, the~~The observed hourly concentrations of air pollutants, including O_3, NO_2, CO, $PM_{2.5}$, and SO_2 from 2015 to 2020 are obtained from the Chinese National Environmental Ministry of Environmental Protection (http://www.cnemc.cn/en/). Gridded MDA8 O_3 data from Tracking Air Pollution in China dataset (http://tapdata.org.cn) with a resolution of 10 km are also used (Xue et al., 2020).

2.2 Meteorological Data

The European Centre for Medium-Range Weather Forecasts (ECMWF) Reanalysis v5 (ERA5) dataset (available at https://cds.climate.copernicus.eu/), with a horizontal resolution of $0.25^\circ \times 0.25^\circ$ and a ~~time interval~~temporal resolution of 1 h, was used to analyze the influence of meteorological parameters on O_3 pollution. The variables used in this study include 2 m temperature (T2m), surface net solar radiation (SSR). In addition, daily mean relative humidity, geopotential height, zonal and meridional wind at 500 hPa, and vertical velocity at 850hPa from the National Center for Environmental Prediction (NCEP) and National Center for Atmospheric Research (NCAR) reanalysis (https://psl.noaa.gov/data/gridded/data.ncep.reanalysis.html) at a resolution of $2.5^\circ \times 2.5^\circ$ are used.

2.3 Methods

The Chinese National Ambient Air Quality Standard for MDA8 O_3 is 160 μg m^{-3}, which corresponds to 75 ppb at 273.15 K and 1 atm. ~~It follows that the~~The O_3-exceeding days are defined as MDA8 O_3 concentration >75 ppb, while non-O_3-exceeding days are defined as MDA8 O_3 concentration <75 ppb. According to the duration of O_3 pollution episode, it can be divided into consecutive O_3-exceeding days with four or more days (O_3 days≥4) and consecutive O_3-exceeding days less than four days (O_3 days<4). In addition, some common statistical methods are used in this study, including linear fitting, meteorological synthesis method, and two-tailed Student's t test.

The normalized annual mean O_3 concentration of the O_3-exceeding days is calculated by adding the O_3 concentration of the O_3-exceeding day each year and dividing it by the total number of days in the year. The normalized annual mean O_3 of the non-O_3-exceeding days is calculated by the same method except for the non-O_3-exceeding days.

Table 1 lists the criteria and corresponding numbers of low O_3 and high O_3 stations in the three megacity clusters. ~~Low O_3 and high O_3 stations are defined basing~~This classification is undertaken with the purpose of distinguishing stations with various O_3 levels within the three megacity clusters, and it is based on the number of O_3 exceeding days in 2015. Stations with the number of O_3-exceeding days fewer than or equal to the low O_3 criterion (second column) are considered as low O_3 stations. When more than or equal to the high O_3 criterion (4th column), they are considered as high O_3 stations. We have tested a few reasonably different criteria and found only some insignificant differences in the results. i.e., the results associated with low O_3 and high O_3 stations are robust against reasonable changes in their selection criteria. For example, the relatively large criterion (37 days) of low O_3 stations in YRD is intended to include a large enough number of stations (about one third of the total of 152 stations) to be fully representative of low O_3 and moderate O_3 stations. These results have been compared to those of a more stringent criterion of nineteen days and found no notable change in the major characteristics (Figs. S1 and S2).

3 Results and discussion

3.1 Major characteristics of O_3 trends

Major characteristics of the large positive trends in the annual mean O_3 concentration are shown in Figs. 2a, 2b and 2c for BTH, YRD and PRD, respectively, in which the normalized annual mean concentrations of MDA8 O_3 in the three megacity clusters are compared to contributions from two groups: The O_3-exceeding days and non-O_3-exceeding days. The increase in O_3-exceeding days is the primary contributor to the substantial increase in the annual mean O_3 in all three megacity clusters from 2015 to 2020. The contribution of O_3-exceeding days is affected mostly by the changing number of exceeding days (more than 80%), and secondly but nevertheless significantly by their changes in concentrations (less than 20%) (Tables 2–4). e.g., in BTH the exceeding days were 31, 43, 62, 74, 96 and 78 days in the individual years of 2015–2020, respectively, while their concentrations of those years were 66.42, 64.13, 69.44, 68.21, 70.19 and 69.69, respectively (Table 2 second column). Contributions from non-O_3-exceeding days are insignificant (p-value > 0.1), except that in BTH (Fig. 2a) which shows a significant declining contribution (p-value = 0.02) due to the reduced number of non-O_3-exceeding days. Therefore, the following discussions on the O_3 trends will be focused on the O_3-exceeding days.

Annual numbers of single and consecutive O_3-exceeding days are shown in Figs. 3a, 3b and 3c for BTH, YRD and PRD, respectively. A drastic two to three-fold increase in the annual numbers of consecutive O_3-exceeding days can be seen in all three regions. In contrast, the numbers of single O_3-exceeding days show only a slight increase in PRD. These drastic increases in the annual numbers of consecutive O_3-exceeding days are clearly the primary contributors to the trends in O_3 shown in Figs. 2a, 2b and 2c. This brings up ~~several~~two key scientific questions: What is the cause(s) of the drastic increases in the numbers of consecutive O_3-exceeding days? Is it due to changing ~~O_3 photochemical processes~~emissions of air pollutants or changing meteorological parameters?

3.2 Spatial expansion and ~~quasi-~~saturation of high O_3

Another important changing characteristics of O_3 concentrations is illustrated in Fig. 4a, which depicts the annual mean concentrations of MDA8 O_3 in BTH during O_3-exceeding days for all 78 stations (black line), 14 stations in the highest category of O_3 concentration (average 103 ppb) observed in 2015 (red line, denoted as high O_3 stations hereafter, Table 1) and 13 stations in the lowest category of O_3 (average 57 ppb) observed in 2015 (green line, denoted as low O_3 stations hereafter, Table 1). It is remarkable that O_3 concentrations at the low O_3 stations caught up within 12 ppb with other stations in merely two years (an increase of about 30 ppb from 2015 to 2017), and actually equaled the average of other stations in 2019. Meanwhile, the high O_3 stations experienced a slight decrease in O_3 concentration, albeit not statistically significant. This phenomenon suggests strongly that the annual mean concentrations of MDA8 O_3 in BTH experienced a fast (within two years) and widespread spatial expansion of high O_3 from urban centers to surrounding regions where O_3 concentrations were low in 2015. Temporally most of the expansion was accomplished during 2015–2017. This phenomenon of a fast and widespread expansion of high O_3 concentrations from urban centers to surrounding regions were also observed at a slightly less degree in YRD (Fig. 4b) and PRD (Fig. 4c).

~~It is worth noting that O_3 concentrations at the high O_3 stations of approximate 100 ppb in 2015 remained nearly constant or slightly declined throughout the entire period of 2015–2020, while the low O_3 stations with O_3 concentrations less than about 75 ppb in 2015 in all three megacity clusters experienced significant enhancements in O_3 concentration (>5 ppb yr^{-1}) during 2015–2017 (Figs. 4a, 4b and 4c). This near-constant O_3 phenomenon suggests a quasi-saturation effect of O_3 formation when the annual mean concentration of MDA8 O_3 reached approximately 100 ppb.~~

Figs. 6a, 6b and 6c are the same as Figs. 5a, 5b and 5c, respectively, ~~except~~but for YRD. Similar to BTH, one can clearly see the expansion of high O_3 from the vicinity of Shanghai City (31 °N, 121.3 °E) in the northwestern direction reaching as far as the central BTH box during the period 2015–2017 (Figs. 6b and 6c). Comparing Fig. 6a to 6b, one can see that the area ~~inside the~~greater than 70-ppb~~ contour~~ expanded from Shanghai and vicinity northwestward by more than a factor of five from 2015 to 2017. This expansion was in different direction from the southwestern expansion occurred in BTH (Fig. 5c). ~~5c). Since it is highly unlikely that any change in emissions could result in these different expansions in YRD and BTH, the logical explanation of the expansion in YRD would be that the weather system conducive to O_3 formation moved from the vicinity of Shanghai in 2015 (Fig. 6a) northwestward toward western BTH in 2017 (~~We note, however, this expansion~~Figs. 6b and 6c). We note, however, this movement of the weather system~~ does not necessarily mean the direct transport of high O_3 or its precursors from the vicinity of Shanghai to central BTH. In fact, the presence of separate rather than contiguous red patches of high O_3 (>70 ppb) in southern BTH and northern YRD in Fig. 6b is a clear indication that the high O_3 are primarily controlled by local photochemical production from local O_3 precursors ~~under the expanded conducive weather conditions~~, rather than the direct upwind-downwind transport of high O_3 and/or its precursors. The daily average concentration of MDA8 O_3 ~~in~~within the YRD box increased from 53.79 ppb in 2015 (31 days, Fig. 6a) to 64.35 ppb in 2017 (40 days, Fig. 6b), which was a difference of 10.56 ppb or a 20% increase between the two years (Fig. 6c). ~~When accounted~~After accounting for the number of O_3-exceeding days, the ratio of normalized MDA8 O_3 in all O_3-exceeding days between 2017 and 2015 became~~:~~

Figs. 7a, 7b and 7c are the same as Figs. 5a, 5b and 5c, respectively, ~~except they are~~but for PRD. Unlike BTH and YRD, there was only a slight expansion of high O_3 within the PRD box toward the southwest in 2017 compared to 2015 (Fig. 7c). Nevertheless, outside the PRD box there was an extensive expansion of high O_3 in eastern China, substantially greater than the expansion within the PRD box (Fig. 7c). The daily average concentration of MDA8 O_3 within the PRD box increased from 61.16 ppb in 2015 (14 days, Fig. 7a) to 65.18 ppb in 2017 (36 days, Fig. 7b), which was a difference of 4.02 ppb or a merely 6.6% increase between the two years (Fig. 7c). After accounting for the number of O_3-exceeding days, the ratio of normalized MDA8 O_3 in all O_3-exceeding days between 2017 and 2015 became 2.74. ~~The calculation formula is:~~This comparison suggests that the increase in O_3 in PRD between 2015 and 2017 was almost entirely (93.4%) due to the increase in the number of O_3-exceeding days.

~~(65.18×36)/(61.16×14)=2.74~~

~~More evidence against the emissions of air pollutants as a major cause of the expansion and quasi-saturation can be seen in Fig. 8, in which the annual mean concentrations of MDA8 O_3 during O_3-exceeding days are compared to those of Ox (O_3+NO_2) as well as other air pollutants in BTH in 2015–2020. The nearly 30 ppb increases in O_3 (Fig. 8a) at low O_3 stations from 2015 to 2017 occurred also in Ox (Fig. 8b), suggesting that titration by NO or emission of NO was not the cause of the increases in O_3 in 2015–2017, even though the titration effect may well be the cause of the smaller overall trend in O_3 during much longer period 2006–2019 as suggested convincingly by Li et al. (2022). In addition, $PM_{2.5}$ concentrations at high O_3 stations in Fig. 8c decreased significantly more than those at low O_3 stations from 2015 to 2017, yet the low O_3 stations experienced a near 30 ppb increase in O_3, while O_3 remained essentially constant at the high O_3 stations, suggesting that the proposed removal of HO_2 radicals by $PM_{2.5}$ (Li K. et al., 2021; Shao et al., 2021) was also not a likely cause of the increases in O_3 in 2015–2017. In this context, it should be pointed out that we do not doubt the validity of HO_2 removal by $PM_{2.5}$, but its effect was obviously too small to impact on the O_3 trend in 2015–2017. Finally, neither CO nor NO_2 showed any notable change at low O_3 stations between 2015 and 2017, implying negligible change in O_3 precursors, NOx and VOCs, as their emission rates tended to be proportional to those of NO_2 and CO, respectively. This again supported the notion that changes in the emissions of O_3 precursors were unlikely to be the driving cause of the increases in O_3 at low O_3 stations from 2015 to 2017.~~

3.3 Cause(s) of the expansion and ~~quasi-~~saturation

Major findings of subsections 3.1 and 3.2 can be summarized as follows: (1) Trends in O_3 observed in the three megacity clusters in eastern China during 2015–2020 (Fig. 1) were mainly caused by the large trends of approximately two to three-fold

带格式的: 下标

increase in the number of consecutive O_3-exceeding days (Figs. 2 and 3). (2) A fast and widespread expansion of high O_3 from urban centers to surrounding regions was observed in the three megacity clusters during 2015–2019 (Fig. 4); and the majority of the expansions were accomplished during the 2015–2017 period (green lines in Fig. 4). And (3~~) The~~), the expansions of high O_3 in the three megacity clusters were accompanied by a ~~quasi-~~saturation effect that O_3 concentrations at the high O_3 stations ~~(high O_3 in 2015)~~ of approximate 100 ppb in 2015 remained nearly constant or slightly declined throughout the entire period of 2015–2020~~, while the low O_3 stations (low O_3 in 2015) with O_3 of about 75 ppb in all three megacity clusters in 2015 experienced significant enhancements in O_3 (>5 ppb yr^{-1}) during 2015–2017 (Figs. 4a, 4b and 4c). And (4) There is independent evidence, including spatial distribution of the expansion (Figs. 5 and 6) and inter-annual variations in O_3, Ox, NO_2, CO and $PM_{2.5}$~~ (Fig. ~~8), suggesting that transport/meteorology rather than emissions of O_3 precursors would more likely be the major cause of the expansion and quasi-saturation. In the following, we explore the evidence in support of changing meteorological parameters as a cause of O_3 trends in 2015–2020.~~4).

3.3.1 Changing emissions as a possible cause of O_3 trends in 2015–2020

As mentioned earlier, two emission oriented hypotheses have been proposed as a possible cause of the O_3 trends in 2015–2020. One is changing emissions of O_3 precursors NOx and VOC (Li et al., 2022). The other is the reduced removal of HO_2 radicals due to diminishing $PM_{2.5}$ suggested by Li K. et al. (2021) and Shao et al. (2021). Li et al. (2022) demonstrated convincingly that the NO titration effect was the cause of the linear trend in O_3 in PRD (0.5 ppb yr^{-1}) during the relatively long period 2006–2019. But for the period 2015–2020, the NO titration effect could account for only about 10% of the linear trend in O_3 of the low O_3 stations in PRD (5.0 ppb yr^{-1}, green line, Fig.S3a).

The increase of 30 ppb in O_3 at the low O_3 stations in BTH from 2015 to 2017 (green line, Fig. 4a and Fig. 8a) represents about 50% increase in O_3. The titration effect can account for only about 5% (Fig. 8f). If this increase of 30 ppb in O_3 were due to an enhancement in O_3 precursors, the enhancement would have to be substantially greater than 50% because of the well-known less-than-linear relationship between changes in O_3 and its precursors, i.e., substantially more percentage changes in precursors are needed for each percentage change in O_3 (Dodge, 1977; Shafer and Seinfeld, 1985). Figs. 8d and 8f show that CO (a proxy for VOC) and NOx changed only by a few percent from 2015 to 2017, more than one order of magnitude less than the changes needed. Hence it appears that changes in meteorological conditions conducive to O_3 formation are more likely the major contributing factor to the 50% increase in O_3 at the low O_3 stations in BTH. Similar argument can be extended to YRD and PRD (Figs. S1 and S3).

The theory of reduced removal of HO_2 radicals by diminishing $PM_{2.5}$ (25%, green line of Fig. 8c) appeared to be valid qualitatively for the 50% increase in O_3 at the low O_3 stations in BTH from 2015 to 2017 (green line of Fig. 8a). But this theory was contradicted directly by the phenomenon at the high O_3 stations where a 30% reduction in $PM_{2.5}$ (red line of Fig. 8c) corresponded to a decrease rather than an increase in O_3 (red line of Fig. 8a).

3.3.2 Changes in meteorological parameters as a possible cause of O_3 trends in 2015–2020

While a specific process/mechanism has yet to be found as the primary contributor to the trends in O_3 observed in the three megacity clusters at this moment, the ~~findings summarized~~discussions above suggest that an examination into transport/meteorological processes involved in O_3 episodes with consecutive O_3-exceeding days could provide useful information on the identity of the primary contributor. Using BTH as an example, we address this issue in the following by dividing O_3 episodes of a given year into two groups: the first group has four or more consecutive O_3-exceeding days (labeled O_3 days≥4), the second group has less than four consecutive O_3-exceeding days (labeled O_3 days<4). Fig.~~Figure~~ 9a shows the mean daily O_3 concentrations of the first group in 2015 (mean concentration of 71.14 ppb inside the BTH box, 7 days), ~~Figure~~Fig. 9b shows the mean daily O_3 concentrations of the second group (65.04 ppb, 24 days), and Fig. 9c is the difference between the two groups (6.10 ppb, Table 2). Figs.~~Figures~~ 9d–9f are the same as Figs. 9a–9c, respectively, ~~except~~but for 2017. The first group in 2017 had 28 days and mean O_3 of 74.43 ppb inside the BTH box, while the second group had 34 days and 65.32 ppb (Table 2). One of the most remarkable differences between 2017 and 2015 in Figs. 9a–9f was the large number of days with four or more consecutive O_3-exceeding days (first group) in 2017 (28 days, Fig. 9d) over that of 2015 (7 days, Fig. 9a), which alone contributed to about 62% of the difference in O_3 between 2017 and 2015 as shown in Fig. 2a (red line). Approximately 30% was contributed by the 10 days' difference (2017 vs. 2015) in the number of days with less than four consecutive O_3-exceeding days (second group). The contribution by the higher average concentration of MDA8 O_3 of the first group in 2017 is only about 8% (Table 2). These values of contributions reconfirm what is shown in Fig. 3a, i.e., the greater frequency of episodes with four or more consecutive O_3-exceeding days contributes the majority (62%) to the higher O_3 in BTH in 2017 vs. 2015, the greater intensity/concentration of O_3 during the episodes contributes only about 8%, consistent with the expansion and ~~quasi-~~saturation effect discussed earlier. The phenomenon of frequency over intensity is even more pronounced when the data of 2015 (4th row and 4th column in Table 2) are compared to those of 2019 (8th row and 4th column in Table 2), in which the higher frequency of the first group of 2019 contributes as much as 83% to the higher O_3 in BTH in 2019 vs. 2015.

The phenomena illustrated in Figs. 9a–9f also exist in YRD and PRD as well as in most other years. Figures equivalent to Figs. 9a–9c for all years in the three city clusters (except PRD during 2015–2016, in which no episode with four or more consecutive O_3-exceeding days occurred) are provided in the Supplementary Material (Figs. ~~S3–S5~~S4–S6). Essential information derived from those figures is summarized in Tables 2–4. The 4th column of Table 2 shows that the number of days with four or more consecutive O_3-exceeding days in BTH increased consistently from 7 days in 2015 to 66 days 2019 ~~and~~but dropped back to 38 days in 2020; this pattern of changes matched very well with those in Fig. 2a (red line). The same can be said for YRD (Table 3) and PRD (Table 4), except there are some minor contributions from the third column in Tables 3 and 4, i.e., days with less than four consecutive O_3-exceeding days. Another remarkable point is that the difference between (>=4days) and (<4days) (5th column) in Tables 2–4 is slightly positive (mostly by a few percent) for all three city clusters in all years, which again implies expansion and ~~quasi-~~saturation of high O_3 in episodes with four or more consecutive O_3-exceeding days. In

带格式的: 英语(美国)

summary, Tables 2–4 show quantitatively that the temporal and spatial changes in O_3 concentrations in three megacity clusters of eastern China during 2015–2020 can be mostly attributed to the changes in the number of days with four or more consecutive O_3-exceeding days. It follows then that the critical question of our quest for the cause(s) of the remarkable large upward linear trend in O_3 of the three megacity clusters becomes: what process/mechanism is conducive to the formation of O_3 episodes with four or more consecutive O_3-exceeding days?

In Figs. 10a and 10b the values of SSR and T2m of the episodes with four or more consecutive O_3-exceeding days are compared to those of O_3 episodes with less than four consecutive O_3-exceeding days, and to those of clean days (non-O_3-exceeding days). As expected, the O_3 episodes with four or more consecutive O_3-exceeding days consistently have the highest values of SSR and T2m, while the clean days have the lowest values. This is the case in nearly all years studied as shown in the Supplementary Material (Fig. ~~S6~~S7) and is also generally true in YRD and PRD (Figs. ~~S7~~S8 and ~~S8~~S9). Coupling the higher values of SSR and T2m in the O_3 episodes with four or more consecutive O_3-exceeding days depicted in Fig. 10 and greater number of days in the O_3 episodes with four or more consecutive O_3-exceeding days shown in Fig. 3, we therefore propose a hypothesis as follows: the cause of worsening O_3 trends in BTH, YRD and PRD from 2015 to 2020 could be attributed to enhanced photochemical O_3 production due to ~~the~~ increased occurrence of meteorological conditions of high solar radiation and positive temperature anomaly at the surface.

Quantitatively the coupling of Fig. 10 with Fig. 3 can be performed by multiplying the difference between the red (four or more consecutive O_3-exceeding days) and green (clean days) values of SSR/T2m in Fig. 10 with the frequency of occurrence (in percentage of total days) of O_3 episodes with four or more consecutive O_3-exceeding days from Fig. 3. The results are compared to the yearly ~~total~~ O_3-exceeding days in Fig. 11. Correlation between the yearly O_3-exceeding days and weighed SSR is very good with R values 0.88 or greater in all three regions, lending strong support for our hypothesis. Correlation between the yearly O_3-exceeding days and weighed T2m is high correlated in BTH but not correlated in YRD and PRD, which probably suggests that T2m is not as strongly coupled to O_3 formation as SSR. Inclusion of O_3 episodes with less than four consecutive O_3-exceeding days in Fig. 11 did not change the correction coefficients significantly, supporting the robustness of results shown in Fig.11.

~~The presence of TCs in the northwest Pacific, specific positions and strengths of WPSH in different regions, and mid-high latitude wave activities can contributed to the increased frequency of meteorological conditions characterized by high solar radiation and positive temperature anomalies at the surface (~~Hu W. et al~~.,~~ . (2023~~; Mao et al., 2020; Ouyang et al., 2022). The contributions of TCs and WPSH are discussed in the following two sections.~~

Mechanically we propose that the O_3 concentrations at the high O_3 stations stayed close to a saturation level of about 100 ppb throughout 2015 to 2020, even under increased downdrafts and stable atmospheric conditions brought about by mid-distance category TCs. This saturation effect was the result of enhanced rates of atmospheric dispersion, dry deposition and photochemical loss at high O_3 concentrations, which were supported by modeling results (Li et al., 2012; Ouyang et al., 2022; Zhang et al., 2023). It is also consistent with theoretical consideration. While the low O_3 stations, where O_3 production were relatively small in 2015, experienced significant enhancements in the O_3 production (32 ppb in BTH, 12 ppb in PRD) from

2015 to 2017 because in the latter year the increased downdrafts and stable atmospheric conditions brought about by mid-distance category TCs were highly conducive to O_3 formation (Hu W. et al., 2023).

Following the analysis by Hu W. et al. (2023), the mean vertical velocity at 850 hPa during all O_3-exceeding days in PRD in 2015 (Fig. 12a) is compared to that of episodes with four or more consecutive O_3-exceeding days in 2017 (Fig. 12b). Major features in Fig. 12 compare very well with those of Fig. 7. E.g., area with positive vertical velocity (downdrafts) in 2017 (red area in Fig. 12b), which was highly conducive to O_3 formation, was by far more widespread and greater in value than that of 2015 (red area in Fig. 12a), agreeing well with the greater high O_3 area of Fig. 7b (2017) than that of Fig. 7a (2015). This agreement confirms that the increase in O_3 in PRD from 2015 to 2017 was caused by increased downdrafts and stable atmospheric conditions (meteorological conditions) brought about by TCs as suggested by Hu W. et al. (2023). The same plots for BTH are shown in Fig. 13. Features of Fig. 13 are highly consistent with those of Fig. 5. The same plot for YRD (Fig. S10) also showed more extensive and greater downdrafts in 2017 than 2015. However, the area of positive vertical velocity in YRD appeared to shift about 500 km to the east compared to the area of high of O_3 in Fig. 6b. Considering the uncertainty in evaluating the vertical velocity and that O_3 formation is also dependent on parameters other than the vertical velocity, the discrepancy is acceptable.

In summary of this section, the trends in O_3 in the three megacity clusters are critically dependent on the number of four or more consecutive O_3-exceeding days. In addition, Hu W. et al. (2023) found that the changing frequency of mid-distance category TCs (i.e., changing meteorological conditions) is the cause of the increases in the numbers of consecutive O_3-exceeding days as well as the O_3 concentrations in PRD. More importantly, our additional analyses of the mean vertical velocity at 850 hPa over the three megacity clusters (Figs. 12, 13 and S10) show that the increases in O_3 in all three megacity clusters from 2015 to 2017 were caused by enhanced downdrafts and stable atmospheric conditions (meteorological conditions) which were highly conducive to O_3 formation. The enhanced downdrafts and stable atmospheric conditions were brought about by TCs and associated WPSH. Here we bring up WPSH because it is well known that the tracks of TCs are influenced strongly by WPSH, and that WPSH affects strongly regional atmospheric dynamics and therefore O_3 formation (Chang et al., 2019; Mao et al., 2020; Ouyang et al., 2022; Zhao and Wang, 2017).

3.3.3 Contribution of ~~WPSH~~western pacific subtropical high

Mao et al. (2020) made a comprehensive study of an 11-day O_3 episode in BTH in 2017 and found it was dominated by the presence of the WPSH and mid-high latitude wave activities. Depending on the position and intensity, WPSH is well known to be a crucial factor affecting O_3 concentrations in various parts of eastern China (Chang et al., 2019; Yin et al., 2019; Zhao and Wang, 2017). During this 11-day O_3 episode, the ridge line of WPSH maintained at approximately 22 °N from June 24 to June 29, which in combination with mid-high latitude wave activities induced meteorological conditions highly conducive to the O_3 production in BTH and northern YRD (Mao et al., 2020).

Following the analysis of Mao et al. (2020), the impact of WPSH on O_3 in BTH in April–September has been analyzed in Fig. ~~12~~14 which depicts the composite 500 hPa geopotential height contours, humidity and winds in BTH in April–September for

O$_3$-exceeding days in 2015 (a), clean days in 2015 (b), O$_3$-exceeding days in 2017 (c), clean days in 2017 (d), O$_3$-exceeding days in 2019 (e) and clean days in 2019 (f). The three years 2015, 2017 and 2019 are chosen because their differences in O$_3$ contribute predominately to the overall O$_3$ trends (Figs. 1–2). The importance of WPSH is clearly visible in all Figs. ~~12a–12f~~14a–14f when the 5880 and 5900 gpm isolines (green lines) of O$_3$-exceeding days are compared to those of clean days. In all three years, the WPSH of the former (O$_3$-exceeding days) were significantly stronger than the latter (clean days) as evident by the strong anticyclonic winds and/or the larger areas inside the 5880 gpm isolines. Even in the case of 2017 when the area inside 5880 gpm isolines of the former looked to be similar to that of the latter, the appearance of 5900 line in the former indicated a stronger WPSH. The strong anticyclonic winds in the ~~former~~O$_3$ exceeding days (Figs. ~~12a, 12c~~14a, 14c and ~~12e~~14e) force moist air of South China Sea northward into southern China and contributed to extensive clouds and precipitation and thus low O$_3$ formation over southern China and southern YRD. This difference in the O$_3$ formation between BTH and southern China provides a good explanation to why the O$_3$-exceeding days mostly occur in different time periods in the three megacity clusters as discussed in Section 3.2. Furthermore, over East China Sea the prevailing westerlies were forced northward, slowed down and lead to meteorological conditions in BTH and northern YRD characterized by cloudless sky, sinking motion and high vertical stability in the lower troposphere, as well as high SSR and positive T2m anomaly at the surface. These meteorological conditions were highly conducive to the formation and accumulation of O$_3$. In contrast, the weaker WPSH of the ~~latter~~clean days allowed relatively strong westerlies to prevail over BTH during clean days in the three years, which tended to disperse O$_3$ (Figs. ~~12b, 12d~~14b, 14d and ~~12f~~14f). e.g., the average wind speed over BTH was about 10 m s^{-1} in Fig. ~~12b~~14b, while only about 5 m s^{-1} in Fig. 12a. Quantitatively Fig. 12c had 31 more O$_3$-exceeding days (93 ppb) than Fig. ~~12a~~14a, the 31 days came at the expense of clean days (52 ppb) (Figs. ~~12b~~14b and ~~12d~~14d). The contribution of these 31 days to the difference in MDA8 O$_3$ between 2017 and 2015 (6.5 ppb, Fig. 1) can be calculated as follows:

带格式的: 字体: Times New Roman

We have made the same analysis for other years as well as for YRD and PRD. The results are mostly similar, and thus presented in the Supplementary material (Figs. ~~S9, S10~~S11, S12 and ~~S11~~S13). Figs.~~13a–13d~~15a–15d for PRD in 2017 and 2019 are shown because there were interesting anticyclonic circulations over PRD during O$_3$-exceeding days in both years (Figs. ~~13a~~15a and ~~13c~~15c). The 2017 anticyclone was a direct product of the WPSH as it resided within the western tip of the 5880 gpm isoline. The 2019 anticyclone was also likely associated with the WPSH as the center of anticyclone resided just beneath the 5860 gpm isoline to the west of PRD. The anticyclonic circulations were accompanied by stable downdrafts, low winds, and cloudless sky conditions (short arrows and blue shades in Figs. ~~13a~~15a and ~~13c~~15c), which were highly conducive to the O$_3$ formation. Cloudless sky conditions also occurred in YRD and BTH in Figs. ~~13a~~15a and ~~13c~~15c, but the high wind speed prevented the accumulation of O$_3$. This difference in O$_3$ accumulation between PRD and other two regions provide another good explanation to why the O$_3$-exceeding days mostly occur in different days in the three megacity clusters as discussed in Section 3.2. Quantitatively Fig. ~~13c~~15c had 27 more O$_3$-exceeding days (90 ppb) than Fig. 13a, the 27 days came at the expense of clean days (39 ppb) (Figs. ~~13b~~15b and ~~13d~~15d). The contribution of these 27 days to the difference in MDA8 O$_3$ in PRD between 2019 and 2017 (6.0 ppb, Fig. 1) can be calculated as follows:

The presence of anticyclonic circulations over PRD is in good agreement with the results of Ouyang et al. (2022) and Hu W. et al. (2023). The latter authors suggested that the anticyclonic circulations over PRD were primarily caused by TCs in northwestern Pacific. Nevertheless, it is widely acknowledged that the tracks of TCs in the northwestern Pacific are influenced, at least to some extent, by WPSH (Sun et al., 2015; Wang et al., 2017), making it difficult to separate the roles played by the TCs on the anticyclonic circulations and O_3 formation from those of WPSH. Clearly, further investigations is needed to fully understand the complex relationship among WPSH, TCs and O_3. Based on these results, we hypothesize that the increased frequency of these meteorological conditions enabled by the changing intensity and position of WPSH could contribute as a major cause of the positive O_3 trends in the three megacity clusters in eastern China during 2015–2020.

3.4 Uncertainty and cautionary statements

带格式的: 字体: 10 磅

It is worth noting that the analyses conducted in Sections 3.1–3.3 have predominantly relied on correlation or regression analysis techniques, which do not imply a cause-and-effect relationship. To establish a cause-and-effect link between the proposed changes in meteorological parameters and O_3 trends, it is necessary to employ a mechanistic model that is based on the proposed causes and can accurately reproduce the observed O_3 trend. Until such model reproduction is achieved, all correlation or regression findings should be considered as a potential maximum cause-and-effect relationship (Wu et al., 2022). However, current mechanistic models suffer from significant uncertainties, making it difficult to credibly simulate critical atmospheric processes that regulate O_3 formation. These processes include atmospheric transport parameterizations, the sources and sinks of OH, HO_2 and RO_2 radicals, and the photochemistry of VOCs and OVOCs.

4 Summary and Conclusions

Thanks to a strong emission control policy, major air pollutants in China, including $PM_{2.5}$, SO_2, NO_2 and CO had shown remarkable reductions during 2015–2020. However, O_3 concentration had increased significantly and emerged as a major air pollutant in eastern China during the same time period. The annual mean concentration of MDA8 in three megacity clusters in eastern China, namely BTH, YRD and PRD, showed alarming large upward linear trends of 25%, 10% and 19%, respectively during 2015–2019. Identifying the causes of these worsening O_3 trends is urgently required for air pollution prevention and management.

Some recent studies suggested that enhanced photochemical processes induced by changing anthropogenic emissions were responsible for these trends (Li et al., 2019; Li et al., 2022; Shao et al., 2021; Wang et al., 2020). However, we noticed that there was independent evidence, including the spatial distribution of the expansion of high O_3 (Figs. 5 and 6) and inter-annual variations in O_3, Ox, NO_2, CO and $PM_{2.5}$ (Fig. 8), suggesting that transport/meteorological conditions rather than emissions of O_3 precursors were more likely to be the major contributor to the O_3 trends. Moreover, we found that the trends in O_3 observed in the three megacity clusters during 2015–2020 (Fig. 1) were mainly caused by the large trend of approximately two to three-fold increase in the number of consecutive O_3-exceeding days (Fig. 3), during that time a fast and widespread expansion of high O_3 from urban centers to surrounding regions was observed (Fig. 4), and the majority of the expansions was accomplished during the two-year 2015–2017 period (green lines in Fig. 4). Furthermore, the expansions of high O_3 in the three megacity clusters were accompanied by a ~~quasi-~~saturation effect that O_3 concentrations at the high O_3 stations (high O_3 in 2015) of approximate 100 ppb remained nearly constant throughout the entire period of 2015–2020, while the low O_3 stations (low O_3 in 2015) with O_3 less than 75 ppb in all three megacity clusters experienced a significant enhancement in O_3 (>5 ppb yr^{-1}) during 2015–2017 (Figs. 4a, 4b and 4c). Finally, greater frequency of episodes with four or more consecutive O_3-exceeding days contributed the majority to the higher O_3 in all three megacity clusters in 2017 vs. 2015, the greater intensity/concentration of O_3 during the episodes contributes only about 10% (Fig. 9), consistent with the expansion and ~~quasi-~~saturation effect discussed earlier.

Coupling the higher values of SSR and T2m in the O_3 episodes with four or more consecutive O_3-exceeding days depicted in Fig. 10 and greater occurrence (number of days) in the O_3 episodes with four or more consecutive O_3-exceeding days shown in Fig. 3, we hypothesize that the cause of the worsening O_3 trends in BTH, YRD and PRD from 2015 to 2020 could be attributed to enhanced photochemical O_3 production due to the increased occurrence of meteorological conditions of high solar radiation and positive temperature anomaly under the influence of WPSH and TCs. The hypothesis is substantiated in Fig. 11, which shows excellent correlation between the yearly O_3-exceeding days and SSR with R values 0.88 or greater in all three regions. Correlation between the yearly O_3-exceeding days and T2m is good in BTH but poor in YRD and PRD, which probably suggests that T2m is not as strongly coupled to O_3 formation as SSR.

~~In conjunction with our study, Hu W. et al. (2023) conducted a statistical analysis to evaluate the processes that promote high O_3 formation in PRD when TCs are present in the northwest Pacific. They assessed the impact of the distance between a TC in the northwest Pacific and PRD on O_3 in the PRD from 2006 to 2020. They found that the increased frequency of the downdrafts and stable atmosphere conditions brought forth by the mid-distance category TCs could be the main cause of the large number of consecutive O_3-exceeding days in 2019, which contribute to about 80% of the overall positive trend of O_3 in 2015–2020 (Fig. 3c and black line, Fig.4c).~~

Therefore, we propose that the O_3 concentrations at the high O_3 stations stayed close to a saturation level of about 100 ppb throughout 2015 to 2020, even under enhanced conditions conducive to O_3 formation, was the result of a relatively high rates of atmospheric dispersion, dry deposition and photochemical loss at the high O_3 concentration. While the low O_3 stations, where O_3 production were relatively small in 2015, experienced significant enhancements in the O_3 production in 2017 and 2019 because of the enhanced downdrafts and stable atmospheric conditions associated with TCs and WPSH in the northwestern Pacific, which were highly conducive to O_3 formation (Hu W. et al., 2023).

Following the analysis of Mao et al. (2020), the impact of WPSH on O_3 in BTH in April–September has been analyzed in Fig. ~~12~~14. We found that the increased frequency of these meteorological conditions enabled by the changing intensity and position of WPSH could contribute as a major cause of the positive O_3 trends in the three megacity clusters in eastern China during 2015–2020.

Nevertheless, it is crucial to recognize that the examinations carried out in Sections 3.1–3.3 primarily utilized correlation or regression analysis techniques, which do not inherently establish causal relationships. To attribute cause and effect between the suggested alterations in meteorological parameters and O_3 trends, it is necessary to employ a mechanistic model that accurately replicates the observed O_3 trend based on the proposed cause(s). Until the model successfully reproduces the phenomenon, all correlation or regression findings should be treated as merely indicating the highest potential cause-and-effect relationship (Wu et al., 2022).

In conclusion, we hypothesize that the cause of the worsening O_3 trends in BTH, YRD and PRD from 2015 to 2020 is attributable to enhanced photochemical O_3 production due to the increased occurrence of meteorological conditions of high solar radiation and positive temperature anomaly under the influence of WPSH and TCs. Therefore, we suggest that future O_3 pollution prevention and control policies should pay more attention to changes in the meteorological/climate conditions, particularly changes in the large-scale circulations, including WPSH and TCs.

Data availability. Hourly surface O_3, NO_2, CO, $PM_{2.5}$, and SO_2 data were obtained from China National Environmental Centre (http://www.cnemc.cn/en/). Hourly meteorological data are obtained from European Centre for Medium-Range Weather Forecasts ERA5 reanalysis (https://cds.climate.copernicus.eu/). Daily meteorological data are obtained from National Center for Environmental Prediction (NCEP) and National Center for Atmospheric Research (NCAR) (https://psl.noaa.gov/data/gridded/data.ncep.reanalysis.html). The data of this study are available upon request to Shaw Chen Liu (shawliu@jnu.edu.cn).

Author Contributions. SL and RL proposed the essential research idea. TH, and YL performed the analysis. TH, YL, RL, and SL drafted the manuscript. YX, BW, and YZ helped analysis and offered valuable comments. All authors have read and agreed to the published version of the manuscript.

Competing interests. The authors declare that they have no conflict of interest.

Acknowledgments. The authors thank the China National Environmental Centre and European Centre for Medium-Range Weather Forecasts for providing datasets that made this work possible. We also acknowledge the support of the Institute for Environmental and Climate Research and Guangdong-Hongkong-Macau Joint Laboratory of Collaborative Innovation for Environmental Quality in Jinan University.

Financial support. This research was supported by the National Natural Science Foundation of China (grant number 92044302, 41805115), Guangzhou Municipal Science and Technology Project, China (grant number 202002020065), Special Fund Project for Science and Technology Innovation Strategy of Guangdong Province (grant number 2019B121205004), Guangdong Innovative and Entrepreneurial Research Team Program (grant number 2016ZT06N263), and National Key Research and Development Program of China (grant number 2018YFC0213906).

References

Bachmann, J. D.: Air quality and climate connections, J. Air Waste Manage., 65, 641–644, https://doi.org/10.1080/10962247.2015.1040697, 2015.

Bell, M. L., Peng, R. D., and Dominci, F.: The exposure–response curve for ozone and risk of mortality and the adequacy of current ozone regulations, Environ. Health Perspect., 114, 532–536, https://doi.org/10.1289/ehp.8816, 2006.

Bian, Y., Huang, Z., Ou, J., Zhong, Z., Xu, Y., Zhang, Z., Xiao, X., Ye, X., Wu, Y., Yin, X., Li, C., Chen, L., Shao, M., and Zheng, J.: Evolution of anthropogenic air pollutant emissions in Guangdong Province, China, from 2006 to 2015, Atmos. Chem. Phys., 19, 11701–11719, https://doi.org/10.5194/acp-19-11701-2019, 2019.

Chang, L., Xu, J., Tie, X., and Gao, W.: The impact of Climate Change on the Western Pacific Subtropical High and the related ozone pollution in Shanghai, China, Sci. Rep., 9, 16998, https://doi.org/10.1038/s41598-019-53103-7, 2019.

Chen, Z., Li, R., Chen, D., Zhuang, Y., Gao, B., Yang, L., and Li, M.: Understanding the causal influence of major meteorological factors on ground ozone concentrations across China, J. Clean. Prod., 242, 118498, https://doi.org/10.1016/j.jclepro.2019.118498, 2020.

Cohen, A. J., Brauer, M., Burnett, R., Anderson, H. R., Frostad, J., Estep, K., Balakrishnan, K., Brunekreef, B., Dandona, L., Dandona, R., Feigin, V., Freedman, G., Hubbell, B., Jobling, A., Kan, H., Knibbs, L., Liu, Y., Martin, R., Morawska, L., Pope III C. A., Shin, H., Straif, K., Shaddick, G., Thomas, M., van Dingenen, R., van Donkelaar, A., Vos, T., Murray, C. J. L., and Forouzanfar, M. H.: Estimates and 25-year trends of the global burden of disease attributable to ambient air pollution: an analysis of data from the Global Burden of Diseases Study 2015, The Lancet, 389, 1907–1918, https://doi.org/10.1016/S0140-6736(17)30505-6, 2017.

Deng, T., Wang, T., Wang, S., Zou, Y., Yin, C., Li, F., Liu, L., Wang, N., Song, L., Wu, C., and Wu, D.: Impact of typhoon periphery on high ozone and high aerosol pollution in the Pearl River Delta region, Sci. Total Environ., 668, 617–630, https://doi.org/10.1016/j.scitotenv.2019.02.450, 2019.

Dodge, M. C.: Effect of selected parameters on predictions of a photochemical model, PB-269858; EPA-600/3-77/048, Environmental Protection Agency, Research Triangle Park, N. C., U.S.A., 1977.

Dong, Y., Li, J., Guo, J., Jiang, Z., Chu, Y., Chang, L., Yang, Y., and Liao, H.: The impact of synoptic patterns on summertime ozone pollution in the North China Plain, Sci. Total Environ., 735, 139559, https://doi.org/10.1016/j.scitotenv.2020.139559, 2020.

Fu, Y., Liao, H., and Yang, Y.: Interannual and decadal changes in tropospheric ozone in China and the associated chemistry-climate interactions: a review, Adv. Atmos. Sci., 36, 975–993, https://doi.org/10.1007/s00376-019-8216-9, 2019.

Gao, D., Xie, M., Chen, X., Wang, T., Liu, J., Xu, Q., Mu, X., Chen, F., Li, S., Zhuang, B., Li, M., Zhao, M., and Ren, J.: Systematic classification of circulation patterns and integrated analysis of their effects on different ozone pollution levels in the Yangtze River Delta Region, China. Atmos. Environ., 242, 117760, https://doi.org/10.1016/j.atmosenv.2020.117760, 2020.

Guo, H., Chen, K., Wang, P., Hu, J., Ying, Q., Gao, A., and Zhang, H.: Simulation of summer ozone and its sensitivity to emission changes in China, Atmos. Pollut. Res., 10, 543–1552, https://doi.org/10.1016/j.apr.2019.05.003, 2019.

Han, H., Liu, J., Shu, L., Wang, T., and Yuan, H.: Local and synoptic meteorological influences on daily variability in summertime surface ozone in eastern China, Atmos. Chem. Physics., 20, 203–222. https://doi.org/10.5194/acp-20-203-2020, 2020.

Hu, W., Liu, R., Chen, Z., Ouyang, S., Hu, T., Wang, Y., Cui, Z., Jiang, B., Chen, D., Liu, S.C., Processes conducive to high ozone formation in Pearl River Delta in the presence of Pacific tropical cyclones, Atoms. Environ., 307, 119859, https://doi.org/10.1016/j.atmosenv.2023.119859, 2023.

Kalabokas, P., Jensen, N.R., Roveri, M., Hjorth, J., Eremenko, M., Cuesta, J., Dufour, G., Foret, G., Beekmann, M.: A study of the influence of tropospheric subsidence on spring and summer surface ozone concentrations at the JRC Ispra station in northern Italy, Atmos. Chem. Phys., 20, 1861–1885, https://doi.org/10.5194/acp-20-1861-2020, 2020.

Lam, Y. F., Cheung, H. M., and Ying, C. C.: Impact of tropical cyclone track change on regional air quality, Sci. Total Environ., 610–611, 1347–1355, https://doi.org/10.1016/j.scitotenv.2017.08.100, 2018.

Li, K., Jacob, D. J., Liao, H., Shen, L., Zhang, Q., and Bates, K. H.: Anthropogenic drivers of 2013–2017 trends in summer surface ozone in China, Proc. Natl. Acad. Sci. U.S.A., 116, 422–427, https://doi.org/10.1073/pnas.181216811, 2019.

Li, K., Jacob, D. J., Liao, H., Qiu, Y., Shen, L., Zhai, S., Bates, K. H., Sulprizio, M. P., Song, S., Lu, X., Zhang, Q., Zheng, B., Zhang, Y., Lee, H. C., and Su, K. K.: Ozone pollution in the North China Plain spreading into the late-winter haze season, Natl. Acad. Sci. U.S.A., 118, e2015797118, https://doi.org/10.1073/pnas.2015797118, 2021.

Li, L., Chen, C. H., Huang, C., Huang, H. Y., Zhang, G. F., Wang, Y. J., Wang, H. L., Lou, S. R., Qiao, L. P., Zhou, M., Chen, M. H., Chen, Y. R., Streets, D. G., Fu, J. S., and Jang, C. J.: Process analysis of regional ozone formation over the Yangtze River Delta, China using the Community Multi-Scale Air Quality modeling system, Atmos. Chem. Phys., 12, 10791–10987. https://doi.org/10.5194/acp-12-10971-2012, 2012.

Li, M., Wang, T., Shu, L., Qu, Y., Xie, M., Liu, J., Wu, H., Kalsoom, U.: Rising surface ozone in China from 2013 to 2017: A response to the recent atmospheric warming or pollutant controls? Atmos. Environ., 246, 118130, https://doi.org/10.1016/j.atmosenv.2020.118130, 2021.

Li, X., Yuan, B., Parrish, D. D., Chen, D., Song, Y., Yang, S., Liu, Z., Shao, M.: Long-term trend of ozone in southern China reveals future mitigation strategy for air pollution, Atmos. Environ., 269, 118869, https://doi.org/10.1016/j.atmosenv.2021.118869, 2022.

Liu, H., Liu, S., Xue, B., Lv, Z., Meng, Z., Yang, X., Xue, T., Yu, Q., and He, K.: Ground-level ozone pollution and its health impacts in China, Atmos. Environ., 173, 223–230, https://doi.org/10.1016/j.atmosenv.2017.11.014, 2018.

Lu, X., Hong, J., Zhang, L., Cooper, O. R., Schultz, M. G., Xu, X., Wang, T., Gao, M., Zhao, Y., and Zhang, Y.: Severe surface ozone pollution in China: A global perspective, Environ. Sci. Technol. Lett., 5, 487–494, https://doi.org/10.1021/ACS.ESTLETT.8B00366, 2018.

Lu, X., Zhang, L., and Shen, L.: Meteorology and climate influences on tropospheric ozone: a review of natural sources, chemistry, and transport patterns, Curr. Pollution Rep., 5, 238–260, https://doi.org/10.1007/s40726-019-00118-3, 2019.

Ma, J., Xu, X., Zhao, C., and Yan, P.: A review of atmospheric chemistry research in China: Photochemical smog, haze pollution, and gas-aerosol interactions, Adv. Atmos. Sci., 29, 1006–1026, https://doi.org/10.1007/s00376-012-1188-7, 2012.

Mao, J., Wang, L., Lu, C., Liu, J., Li, M., Tang, G., Ji, D., Zhang, N., and Wang, Y.: Meteorological mechanism for a large-scale persistent severe ozone pollution event over eastern China in 2017, J. Environ. Sci., 92, 187–199, https://doi.org/10.1016/j.jes.2020.02.019, 2020.

Monks, P. S., Archibald, A. T., Colette, A., Cooper, O., Coyle, M., Derwent, R., Fowler, D., Granier, C., Law, K. S., Mills, G. E., Stevenson, D. S., Tarasova, O., Thouret, V., von Schneidemesser, E., Sommariva, R., Wild, O., and Williams, M. L.: Tropospheric ozone and its precursors from the urban to the global scale from air quality to short-lived climate forcer, Atmos. Chem. Phys., 15, 8889–8973, https://doi.org/10.5194/acp-15-8889-2015, 2015.

Nuvolone, D., Petri, D., and Voller, F.: The effects of ozone on human health, Environ. Sci. Pollut. Res. Int., 25, 8074–8088, https://doi.org/10.1007/s11356-017-9239-3, 2018.

Ouyang, S., Deng, T., Liu, R., Chen, J., He, G., Leung, J. C.-H., Wang, N., and Liu, S. C.: Impact of a subtropical high and a typhoon on a severe ozone pollution episode in the Pearl River Delta, China, Atmos. Chem. Phys., 22, 10751–10767, https://doi.org/10.5194/acp-22-10751-2022, 2022.

Professional Committee of Ozone Pollution Control of Chinese Society for Environmental Sciences: The Bluebook: Prevention and Control of Ozone Pollution in China (2020), Science Press, Beijing, China, ISBN 978-7-03-071664-4, 2022 (in Chinese).

Rowlinson, M. J., Rap, A., Arnold, S. R., Pope, R. J., Chipperfield, M. P., McNorton, J., Forster, P., Gordon, H., Pringle, K. J., Feng, W., Kerridge, B. J., Latter, B. L., and Siddans, R.: Impact of El Niño–Southern Oscillation on the interannual variability of methane and tropospheric ozone, Atmos. Chem. Phys., 19, 8669–8686, https://doi.org/10.5194/acp-19-8669-2019, 2019.

Shafer, T. B., and Seinfeld, J. H.: Evaluation of chemical reaction mechanisms for photochemical smog. Part 3. Sensitivity of EKMA (Empirical Kinetic Modeling Approach) to chemical mechanism and input parameters. Final Report, March 1984–February 1985, PB-85-210888/XAB, California Institute of Technology, Pasadena, U.S.A., 1985.

Shao, M., Wang, W., Yuan, B., Parrish, D. D., Li, X., Lu, K., Wu, L., Wang, X., Mo, Z., Yang, S., Peng, Y., Kuang, Y., Chen, W., Hu, M., Zeng, L., Su, H., Cheng, Y., Zheng, J., and Zhang, Y.: Quantifying the role of $PM_{2.5}$ dropping in variations of ground-level ozone: Inter-comparison between Beijing and Los Angeles, Sci. Total Environ., 788, 147712, https://doi.org/10.1016/j.scitotenv.2021.147712, 2021.

Sun, Y., Zhong, Z., Yi, L., Li, T., Chen, M., Wan, H., Wang, Y., and Zhong, K.: Dependence of the relationship between the tropical cyclone track and western Pacific subtropical high intensity on initial storm size: A numerical investigation. J. Geophys. Res. Atmos., 120(22), 11451–11467, https://doi.org/10.1002/2015jd023716, 2015.

Wang, T., Xue, L., Brimblecombe, P., Lam, Y. F., Li, L., and Zhang, L.: Ozone pollution in China: A review of concentrations, meteorological influences, chemical precursors, and effects, Sci. Total Environ., 575, 1582–1596, https://doi.org/10.1016/j.scitotenv.2016.10.081, 2017.

Wang, Y., Gao, W., Wang, S., Song, T., Gong, Z., Ji, D., Wang, L., Liu, Z., Tang, G., Huo, Y., Tian, S., Li, J., Li, M., Yang, Y., Chu, B., Petäjä, T., Kerminen, V.-M., He, H., Hao, J., Kulmala, M., Wang, Y., and Zhang, Y.: Contrasting trends of $PM_{2.5}$ and surface-ozone concentrations in China from 2013 to 2017, Natl. Sci. Rev., 7, 1331–1339, https://doi.org/10.1093/nsr/nwaa032, 2020.

Wei, X., Lam, K.-S., Cao, C., Li, H., and He, J.: Dynamics of the Typhoon Haitang related high ozone episode over Hong Kong, Adv. Meteorol., 6089154, https://doi.org/10.1155/2016/6089154, 2016.

Wu, Y., Liu, R., Li, Y., Dong, J., Huang, Z., Zheng, J., and Liu. S. C.: Contributions of meteorology and anthropogenic emissions to the trends in winter $PM_{2.5}$ in eastern China 2013–2018, Atmos. Chem. Phys., 22, 11945–11955, https://doi.org/10.5194/acp-22-11945-2022, 2022.

Xue, T., Zheng, Y., Geng, G., Xiao, Q., Meng, X., Wang, M., Li, X., Wu, N., Zhang, Q., and Zhu, T.: Estimating spatiotemporal variation in ambient ozone exposure during 2013–2017 using a data-fusion model, Environ. Sci. Technol., 54, 14877–14888, https://doi.org/10.1021/acs.est.0c03098, 2020.

Yang, W., Chen, H., Wang, W., Wu, J., Li, J., Wang, Z., Zheng, J., and Chen, D.: Modeling study of ozone source apportionment over the Pearl River Delta in 2015, Environ. Pollut., 253, 393–402, https://doi.org/10.1016/j.envpol.2019.06.091, 2019.

Yang, Y., Liao, H., and Li, J.: Impacts of the East Asian summer monsoon on interannual variations of summertime surface-layer ozone concentrations over China, Atmos. Chem. Phys., 14, 6867–6879, https://doi.org/10.5194/acp-14-6867-2014, 2014.

Yin, Z., Cao, B., and Wang, H.: Dominant patterns of summer ozone pollution in eastern China and associated atmospheric circulations, Atmos. Chem. Phys., 19, 13933–13943, https://doi.org/10.5194/acp-19-13933-2019, 2019.

Zhai, S., Jacob, D. J., Wang, X., Shen, L., Li, K., Zhang, Y., Gui, K., Zhao, T., and Liao, H.: Fine particulate matter ($PM_{2.5}$) trends in China, 2013–2018: separating contributions from anthropogenic emissions and meteorology, Atmos. Chem. Phys., 19, 11031– 11041, https://doi.org/10.5194/acp-19-11031-2019, 2019.

Zhang, Y., Tao, M., Zhang, J., Liu, Y., Chen, H., Cai, Z., and Konopka, P.: Long-term variations in ozone levels in the troposphere and lower stratosphere over Beijing: observations and model simulations, Atmos. Chem. Phys., 20, 13343–13354, https://doi.org/10.5194/acp-20-13343-2020, 2020.

Zhang, R.: Relations of water vapor transport from Indian Monsoon with that over East Asia and the summer rainfall in China. Adv. Atmos. Sci. 18 (5), 1005–1017, http://doi.org/10.1007/bf03403519, 2001.

Zhang, S., Zhang, Z., Li, Y., Du, X., Qu, L., Tang, W., Xu, J. and Meng, F.: Formation processes and source contributions of ground-level ozone in urban and suburban Beijing using the WRF-CMAQ modelling system, J. Environ. Sci., 127, 753–766, https://doi.org/10.1016/j.jes.2022.06.01, 2023.

Zhao, W., LÜ, M., Lu, Q., Gao, B., Liang, X., Liu, M., Sun, J., Chen, L., and Fan, S.: Effects of tropical cyclones on ozone pollution in the Pearl River Delta in autumn, Environ. Sci., 43, 2957–2965, https://doi.org/10.13227/j.hjkx.202109169, 2022 (in Chinese).

Zhao, Z. and Wang, Y.: Influence of the West Pacific subtropical high on surface ozone daily variability in summertime over eastern China, Atmos. Environ., 170, 197–204, https://doi.org/10.1016/j.atmosenv.2017.09.024, 2017.

Zheng, B., Tong, D., Li, M., Liu, F., Hong, C., Geng, G., Li, H., Li, X., Peng, L., Qi, J., Yan, L., Zhang, Y., Zhao, H., Zheng, Y., He, K., and Zhang, Q.: Trends in China's anthropogenic emissions since 2010 as the consequence of clean air actions, Atmos. Chem. Phys., 18, 14095–14111, https://doi.org/10.5194/acp-18-14095-2018, 2018.

Table 1. Criteria and corresponding numbers of low O_3 and high O_3 stations in the three megacity clusters in 2015. The criterion listed for each megacity cluster was based on the number of MDA8 O_3 exceeding days in 2015. For instance, the criterion for a low O_3 site in BTH was the number of MDA8 O_3 exceeding days in 2015 being less than or equal to 19 days, while for high O_3 site was the number of MDA8 O_3 exceeding days in 2015 being greater than or equal to 71 days.

	Criterion of low O_3 stations	Number of low O_3 stations	Criterion of high O_3 stations	Number of high O_3 stations	Total number of stations
BTH	≤ 19 days	13	≥ 71 days	14	78
YRD	≤ 37 days	54	≥ 67 days	13	152
PRD	≤ 12days	10	≥ 46 days	10	48

Table 2. Mean O_3 concentrations (ppb) and number of days of all O_3-exceeding days (2nd column), consecutive O_3-exceeding days with less than four days (3rd column), consecutive O_3-exceeding days with four or more days (4th column) and the difference between (≥4days) and (<4days) (5th column) within the BTH box in 2015–2020.

	All days Concentration (days) ppb	<4 days Concentration (days) ppb	≥4 days Concentration (days) ppb	Difference (≥4 days) – (<4 days) ppb
2015	66.42(31)	65.04(24)	71.14(07)	6.10
2016	64.13(43)	62.65(26)	66.39(17)	3.74
2017	69.44(62)	65.32(34)	74.43(28)	9.11
2018	68.21(74)	65.43(27)	69.80(47)	4.37
2019	70.19(96)	65.28(30)	72.42(66)	7.14
2020	69.69(78)	65.52(40)	74.08(38)	8.56

Table 3. ~~Same as Table 2, but for YRD~~Mean O_3 concentrations (ppb) and number of days of all O_3-exceeding days (2nd column), consecutive O_3-exceeding days with less than four days (3rd column), consecutive O_3-exceeding days with four or more days (4th column) and the difference between (≥4days) and (<4days) (5th column) within the YRD box in 2015–2020.

	All days	<4 days	≥4 days	Difference
	Concentration (days) ppb	Concentration (days) ppb	Concentration (days) ppb	(≥4 days) – (<4 days) ppb
2015	53.79(31)	53.59(19)	54.11(12)	0.52
2016	58.87(27)	58.03(23)	63.73(04)	5.70
2017	64.35(40)	62.62(25)	67.22(15)	4.60
2018	63.33(43)	62.49(32)	65.75(11)	3.26
2019	67.18(49)	66.09(27)	68.51(22)	2.42
2020	65.84(38)	64.12(27)	70.06(11)	5.94

Table 4. ~~Same as Table 2, but for PRD~~Mean O_3 concentrations (ppb) and number of days of all O_3-exceeding days (2nd column), consecutive O_3-exceeding days with less than four days (3rd column), consecutive O_3-exceeding days with four or more days (4th column) and the difference between (≥4days) and (<4days) (5th column) within the PRD box in 2015–2020.

	All days Concentration (days) ppb	<4 days Concentration (days) ppb	≥4 days Concentration (days) ppb	Difference (≥4 days) – (<4 days) ppb
2015	61.16(14)	61.16(14)	---(0)	---
2016	58.44(19)	58.44(19)	---(0)	---
2017	65.18(36)	64.60(23)	66.20(13)	1.60
2018	65.82(31)	63.27(16)	68.55(15)	5.28
2019	69.80(62)	65.96(29)	73.16(33)	7.20
2020	65.08(37)	63.87(22)	66.84(15)	2.97

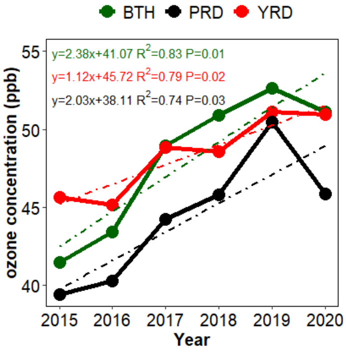

Figure 1: Annual mean concentrations of maximum daily 8-hour average O_3 in BTH (green), YRD (red) and PRD (black).

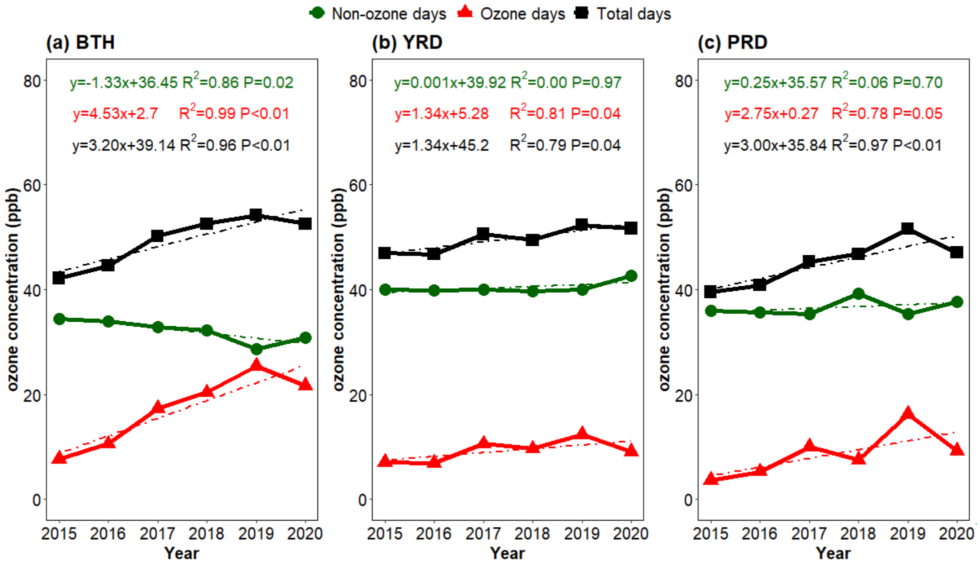

Figure 2: Contributions from the O_3-exceeding days (red) and non-O_3-exceeding days (green) to the annual mean concentration of maximum daily 8-hour average O_3 (black) in BTH (a), YRD (b) and PRD (c).

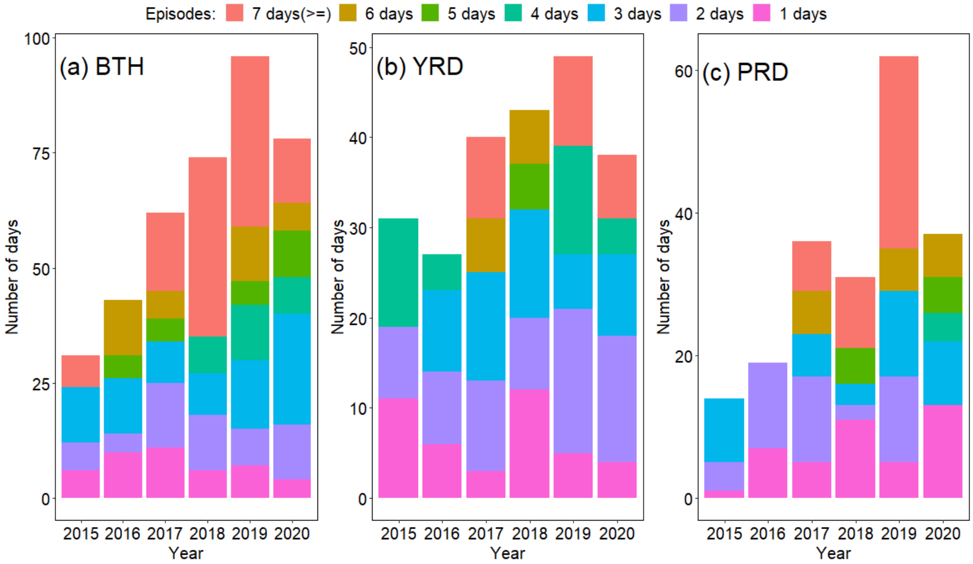

Figure 3: Annual numbers of various consecutive O_3-exceeding days in BTH (a), YRD (b) and PRD (c). Individual colors denote different numbers of consecutive O_3-exceeding days.

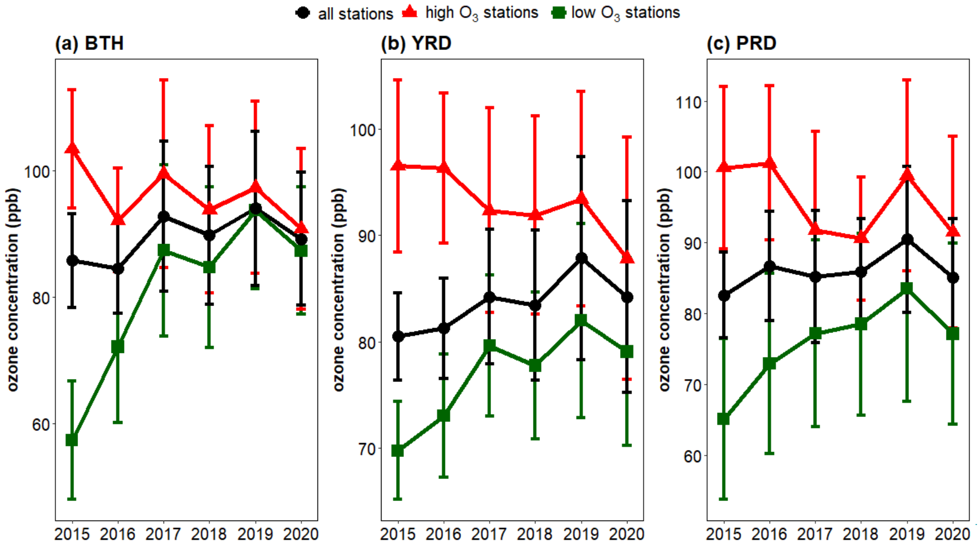

Figure 4: Mean concentrations of maximum daily 8-hour average O_3 during O_3-exceeding days for all stations (black), high O_3 stations (red) and low O_3 stations (green) in BTH (a), YRD (b) and PRD (c).

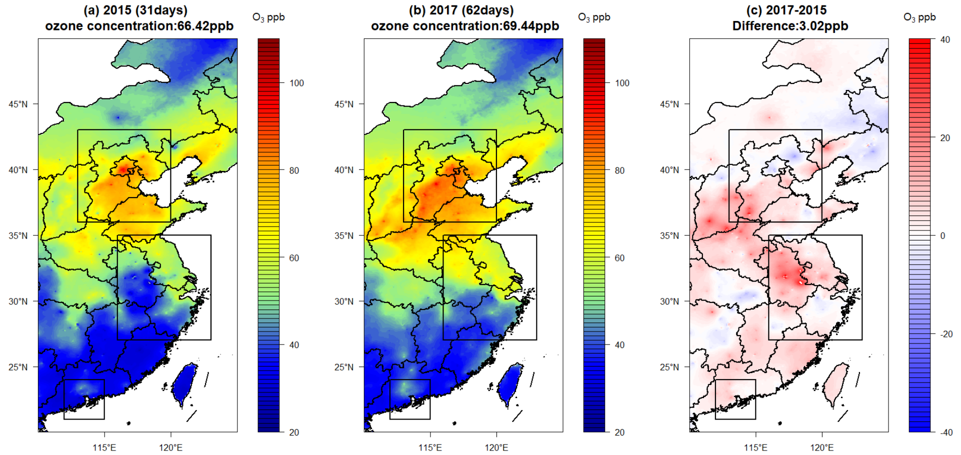

Figure 5: Spatial distribution of annual mean concentrations of maximum daily 8-hour average O_3 for O_3-exceeding days in BTH in 2015 (a), 2017 (b) and their difference (2017 - 2015) (c). The top, middle and bottom rectangle boxes denote BTH, YRD and PRD districts, respectively. The number inside the parenthesis behind 2015 or 2017 denotes the number of O_3-exceeding days.

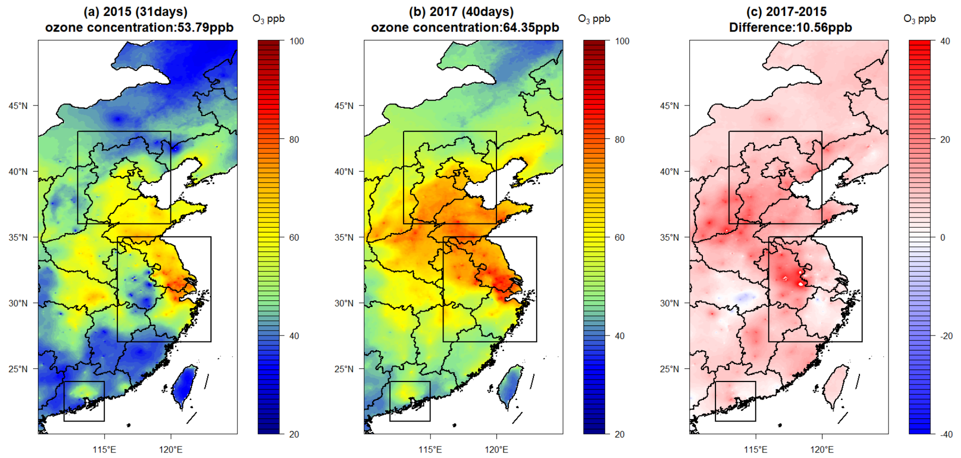

Figure 6: Spatial distribution of annual mean concentrations of maximum daily 8-hour average O$_3$ for O$_3$-exceeding days in YRD in 2015 (a), 2017 (b) and their difference (2017 - 2015) (c). The top, middle and bottom rectangle boxes denote BTH, YRD and PRD districts, respectively. The number inside the parenthesis behind 2015 or 2017 denotes the number of O$_3$-exceeding days.

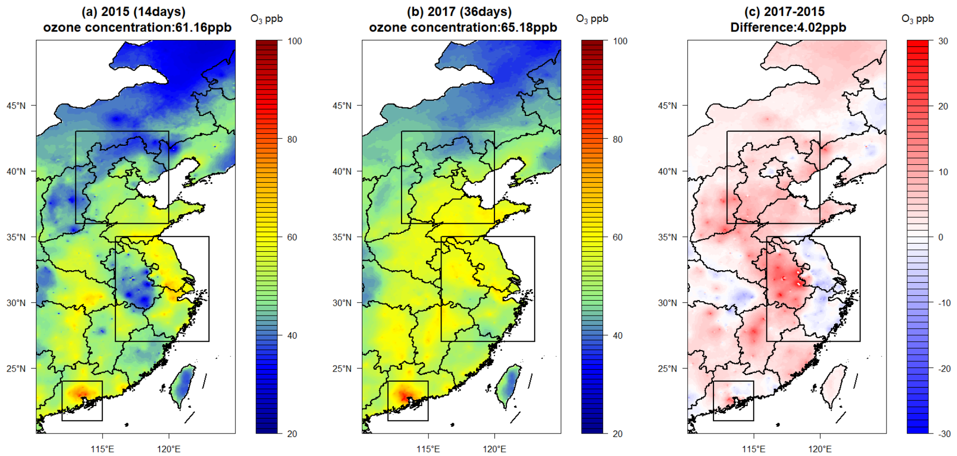

Figure 7: Spatial distribution of annual mean concentrations of maximum daily 8-hour average O_3 for O_3-exceeding days in PRD in 2015 (a), 2017 (b) and their difference (2017 - 2015) (c). The top, middle and bottom rectangle boxes denote BTH, YRD and PRD districts, respectively. The number inside the parenthesis behind 2015 or 2017 denotes the number of O_3-exceeding days.

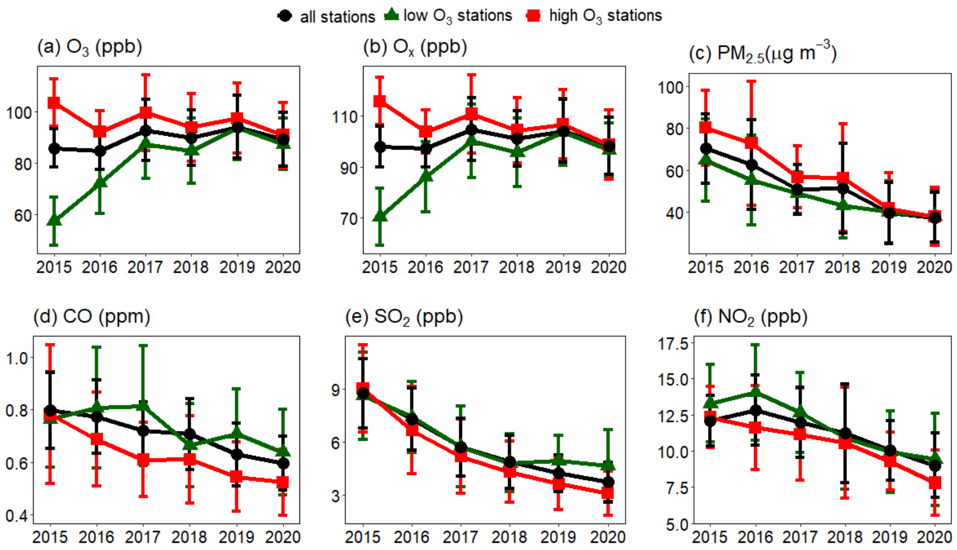

Figure 8: Annual mean concentrations of maximum daily 8-hour average O_3 in BTH during O_3-exceeding days for all stations (black), high O_3 stations (red) and low O_3 stations (green) (a), same as (a) ~~except~~but for Ox (b), $PM_{2.5}$ (c), CO (d), SO_2 (e), NO_2 (f).

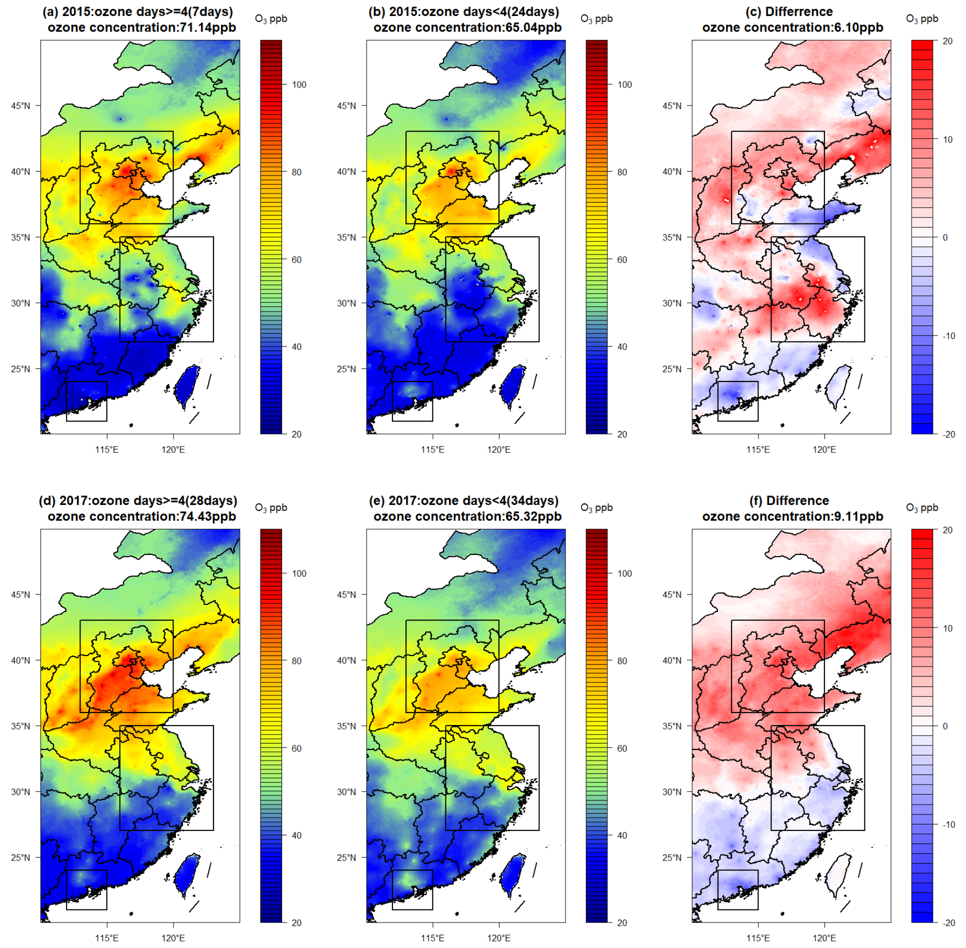

Figure 9: Spatial distribution of daily mean MDA8 O_3 of O_3-exceeding days in BTH for O_3 episodes with four or more consecutive O_3-exceeding days in 2015 (a), O_3 episodes with less than four consecutive O_3-exceeding days in 2015 (b), and (a minus b) (c); (d, e and f) are the same as (a, b and c), respectively, ~~except~~but for 2017.

655

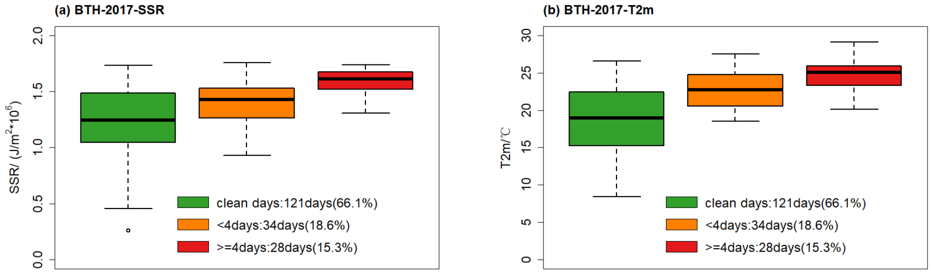

Figure 10: Surface solar radiation (SSR) (a) and temperature (T2m) (b) in BTH in April–September 2017 for four episodes with four or more consecutive O_3-exceeding days (red), clean days (non-O_3-exceeding days) (green) and O_3 episodes with less than four consecutive O_3-exceeding days (orange).

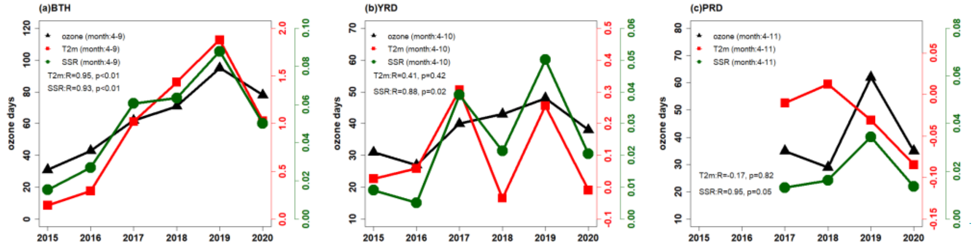

Figure 11~~.~~: Correlations among annual O_3-exceeding days, surface solar radiation (SSR) and temperature (T2m) in BTH (a), YRD (b) and PRD (c).

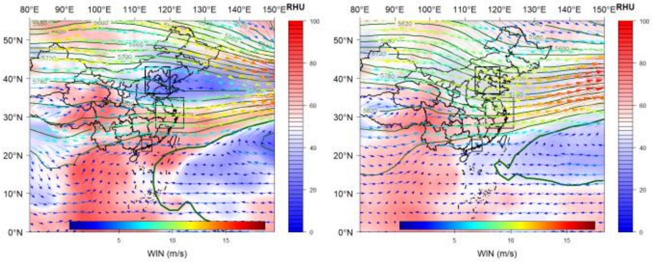

(a) 2015：all O_3 days

(86ppb, 31 days)

(b) 2015：clean days

(52ppb, 152 days)

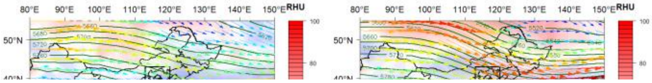

(c) 2017：all O_3 days

(93ppb, 62 days)

(d) 2017：clean days

(56ppb, 121 days)

Figure 12: Mean vertical velocity at 850hPa during O_3-exceeding days in PRD in 2015 (a) and during episodes with four or more consecutive O_3-exceeding days in 2017 (b).

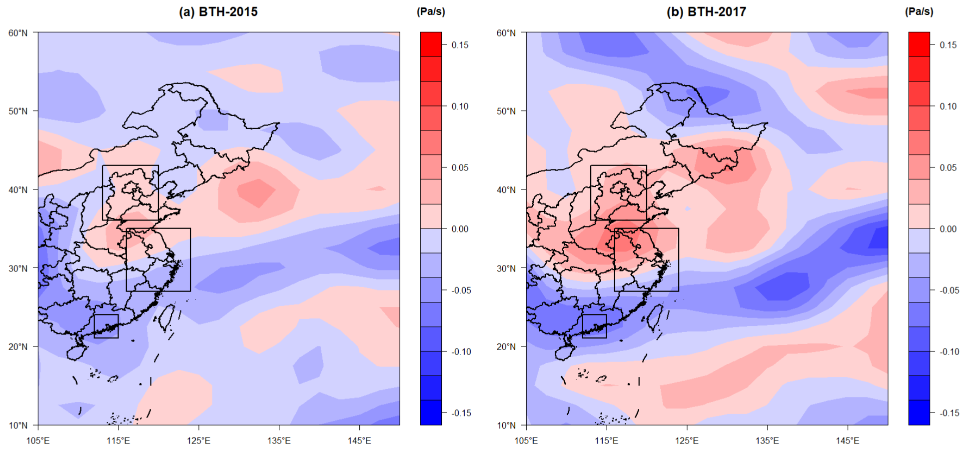

Figure 13: Mean vertical velocity at 850 hPa during O_3-exceeding days in BTH in 2015 (a) and during episodes with four or more consecutive O3-exceeding days in 2017 (b).

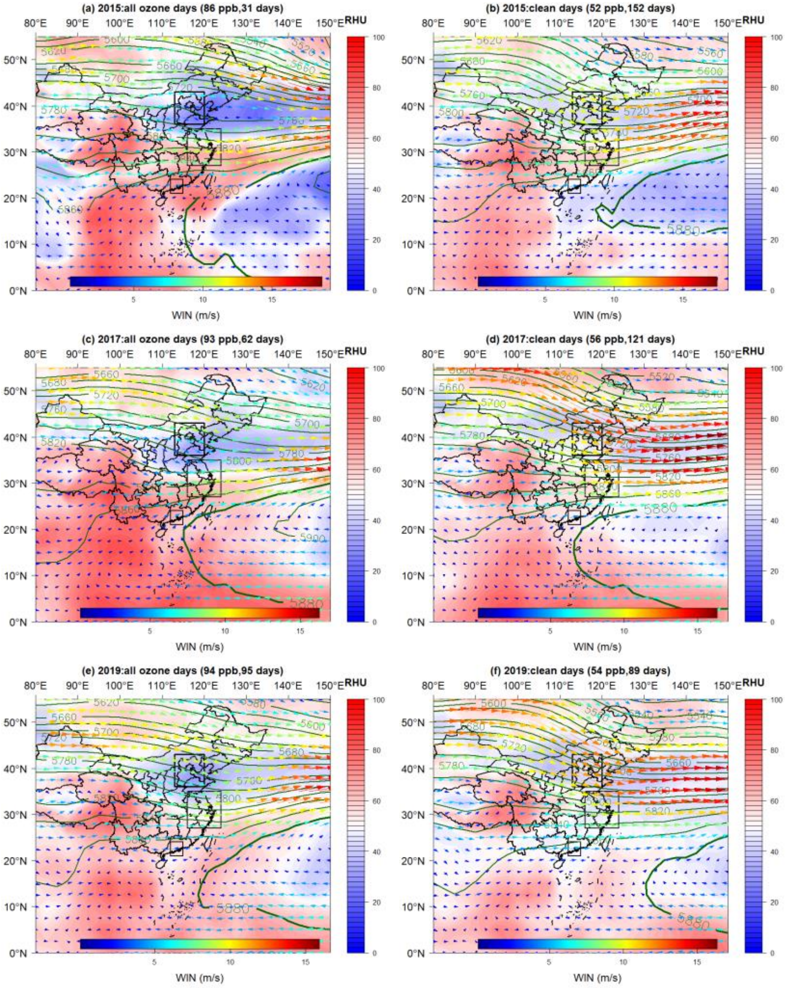

(a) 2015:all ozone days (86 ppb,31 days)

(b) 2015:clean days (52 ppb,152 days)

(c) 2017:all ozone days (93 ppb,62 days)

(d) 2017:clean days (56 ppb,121 days)

(e) 2019:all ozone days (94 ppb,95 days)

(f) 2019:clean days (54 ppb,89 days)

Figure 14: Composite 500 hPa geopotential height contours, humidity and winds in BTH in April-September for O_3-exceeding days in 2015 (a), clean days in 2015 (b), O_3-exceeding days in 2017 (c), clean days in 2017 (d), O_3-exceeding days in 2019 (e) and clean days in 2019 (f).

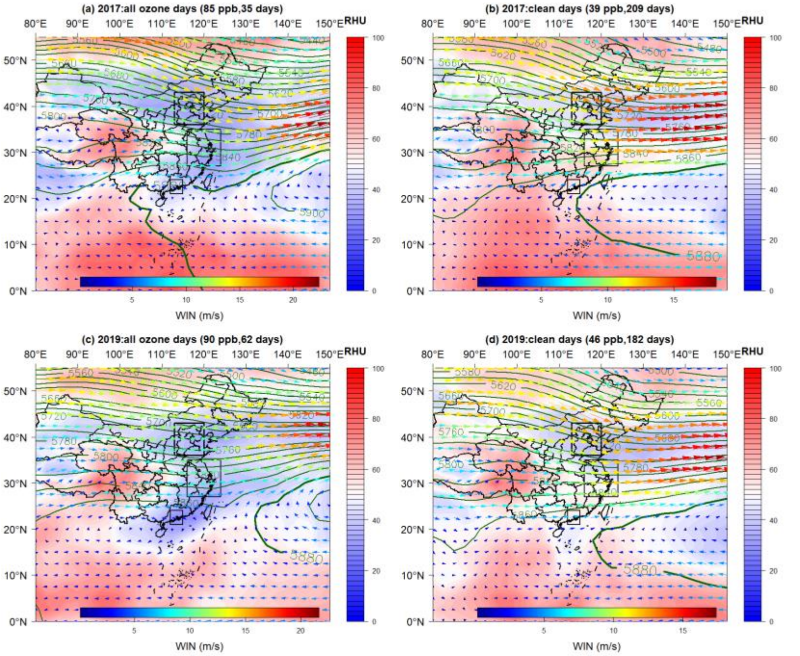

Figure ~~13~~15: Composite 500 hPa geopotential height contours, humidity and winds in PRD in April-November for O_3-exceeding days in 2017 (a), clean days in 2017 (b), O_3-exceeding days in 2019 (c), clean days in 2019 (d).